Science of the Total Environment 633 (2018) 677–683

Contents lists available at ScienceDirect

Science of the Total Environment

journal homepage: www.elsevier.com/locate/scitotenv

Filling the missing data gaps of daily MODIS AOD using spatiotemporal interpolation

Jing Yang [a,b,1], Maogui Hu [a,c,*,1]

[a] State Key Laboratory of Resources and Environmental Information System, Institute of Geographic Sciences and Natural Resources Research, CAS, Beijing 100101, China
[b] University of Chinese Academy of Sciences, Beijing 100049, China
[c] Jiangsu Center for Collaborative Innovation in Geographical Information Resource Development and Application, Nanjing 210023, China

HIGHLIGHTS

- We produced a gap-filling daily MODIS AOD product based on spatiotemporal kriging.
- The completeness of product was significantly improved from 14.27% to 67.73%.
- The spatiotemporal kriging performed better and more stable than spatial kriging interpolation method.
- The AOD distribution in Beijing had typical seasonal variations that were highly related to topography.

GRAPHICAL ABSTRACT

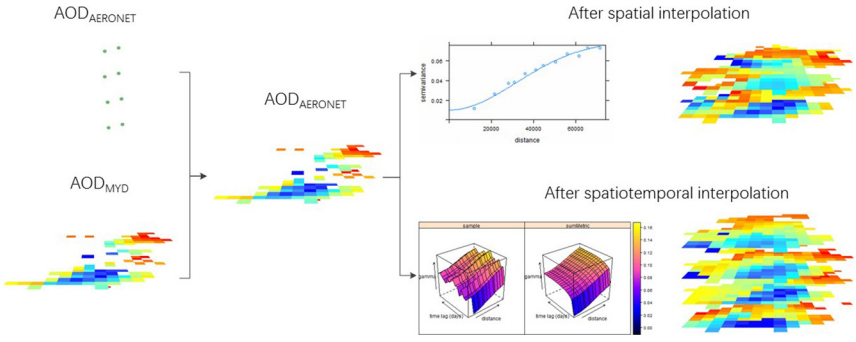

ARTICLE INFO

Article history:
Received 7 November 2017
Received in revised form 15 March 2018
Accepted 18 March 2018
Available online 28 March 2018

Editor: Jianmin Chen

Keywords:
MODIS aerosol product
Spatiotemporal correlation
Missing AOD data
Interpolation

ABSTRACT

Aerosol is an important component of the atmosphere that affects the environment, climate, and human health. Remote sensing is an efficient observation method for monitoring global aerosol distribution and changes over time. The daily Moderate Resolution Imaging Spectroradiometer (MODIS) level-2 aerosol optical depth (AOD) (Collection 6) product (10 km resolution) is often used to study climate change and air pollution. However, the product is prone to yielding large amounts of data gaps due to the unfeasibility of retrieving reliable estimates under cloudy conditions, and these data gaps inevitably affect the results and analysis of the product's application. In this study, a geostatistical data interpolation framework based on the spatiotemporal kriging method was implemented to interpolate satellite AOD products in Beijing, China. Compared to the ordinary kriging method for filling data gaps, the spatiotemporal interpolation not only utilizes spatial autocorrelation but also considers the temporal and spatiotemporal autocorrelations between different locations. In the study region, the completeness of the spatiotemporal-interpolated AOD product reaches 67.73%, which is significantly superior to the completeness of the original MODIS product (14.27%) and that of the spatial kriging-interpolated AOD product (33.3%). The cross-validation results show that the mean absolute error of the spatiotemporal kriging results (0.07) is lower than that of the ordinary kriging (0.09).

© 2018 Elsevier B.V. All rights reserved.

* Corresponding author at: State Key Laboratory of Resources and Environmental Information System, Institute of Geographic Sciences and Natural Resources Research, CAS, Beijing 100101, China.
E-mail address: humg@lreis.ac.cn (M. Hu).
[1] Authors contributed equally to this work.

https://doi.org/10.1016/j.scitotenv.2018.03.202
0048-9697/© 2018 Elsevier B.V. All rights reserved.

1. Introduction

Aerosols are solid and/or liquid particles suspended in the air, such as dust, smoke, and haze (Chin, 2009). Both natural and human processes contribute to aerosol concentrations, which directly and indirectly affect climate (Flato et al., 2013). The direct effect of aerosols on climate involves scattering and absorption of radiation, while the indirect effect occurs by modifying the optical properties and lifetimes of clouds (Ramachandran, 2007). In fact, radiation changes in the earth's climate system do not always lead to global warming; aerosol is also the main factor in global cooling (Chin, 2009). Aerosol loading, or the amount of aerosol in the atmosphere, is usually quantified by mass concentration or by an optical measure, such as aerosol optical depth (AOD), which is the vertical integral of aerosol extinction coefficients along the entire height of the atmosphere (Tang et al., 2016).

The AOD can be determined using satellite-based observations and ground-based observations (Chen et al., 2016). The Aerosol Robotic Network (AERONET) is one of the most important ground-based aerosol monitoring networks in the world and provides reliable temporal continuous AOD values. However, because of the limited number of monitoring sites, it is difficult to carry out a regional, small-scale area analysis (Liu et al., 2004). Satellite-based observations, such as the Moderate Resolution Imaging Spectroradiometer (MODIS), have been widely used in the study of aerosol radiative forcing to monitor regional and global climate because of their high spatial resolution and global coverage, which sufficiently make up for the sparsely distributed ground-monitoring sites of the AERONET (Qi et al., 2013). However, the satellite AOD algorithm relies on specific conditions, such as the absence of clouds: if the satellite is covered by clouds, then it will produce more data gaps (Kokhanovsky et al., 2007). When relying on appropriate surface conditions under dark conditions, the inversion results will be poor in the desert or near the coast (Remer et al., 2005). These large numbers of data gaps limit the applicability of the product to air quality monitoring and forecasting.

Several researchers have attempted to fill the AOD data gaps by fusing datasets from different sources. Other researchers have calculated the monthly mean or used scale coarsening to ignore the data gaps (Chatterjee et al., 2010; Chen and Tian, 2010; Papadimas et al., 2008). However, ignoring the data gaps may result in inaccurate analysis, especially in high-concentration areas. Although some scholars have proposed a variety of cloud removal algorithms for satellite-based observations, information on aerosol in thick clouds tends to be difficult to retrieve due to the instability of the aerosol distribution in such clouds (Sahoo and Patnaik, 2008). Several attempts have been made to merge multi-sensor AOD. Singh et al. (2016) developed an interpolated AOD product based on MODIS and Multi-angle Imaging SpectroRadiometer (MISR) AOD datasets using a Bayesian model. However, the spatial resolution of the interpolated AOD dataset was 0.25° × 0.25°, and this resolution value makes it difficult to meet fine-scale air quality monitoring needs. Tang et al. (2016) developed a spatiotemporal, statistical data fusion framework based on the Bayesian maximum entropy method. The mean spatiotemporal completeness of AOD was improved to 95.2%, and the validation results were also rather good. However, the large computation requirement may limit its application in large areas and long time series. Ruiz-Arias et al. (2013) presented a geostatistical methodology for reducing bias and removing data gaps for a daily gridded AOD dataset with a resolution of 1° × 1°. Van Donkelaar et al. (2010) developed an approach for combining MODIS and MISR AOD into a single improved estimate of AOD. Chatterjee et al. (2010) applied the universal kriging method to average AOD from MISR, MODIS, and AERONET to achieve high-precision AOD products. Although the spatial interpolation method works rather well, temporal correlation was not considered in the research. Actually, similar to meteorological elements (Hengl et al., 2012), AOD distribution can be treated as a typical spatiotemporal random field. An efficient spatiotemporal AOD gap-filling model that contains different aspects of correlation and requires considerable computation is necessary for applications in large areas.

In this study, we present a procedure to interpolate daily MODIS level-2 AOD (Collection 6) over a one-year period using the spatiotemporal (ST) kriging method. The MODIS level-2 AOD product files of the Beijing area for the entire calendar year of 2014 were collected from both the Terra and Aqua satellites. First, we examined the correlation between the MODIS AOD and the AERONET AOD. After that, we calibrated the former data with that of the latter using a linear regression model. Then, the calibrated MODIS AOD data was modeled using the spatiotemporal kriging method. Finally, the results of the interpolation were validated by 10-fold cross validation and compared with the results of the spatial ordinary kriging (OK) method.

2. Data and methods

2.1. Study area

Beijing is the political and cultural center of China, with a population of >21.5 million (Zhang and Wu, 2018). The north and west of Beijing are surrounded by mountains, which means that Beijing is in a "dust-pan" pocket. When monsoons occur in the southeast, the atmosphere in the region does not circulate easily. Moreover, the city is surrounded by large numbers of industrial exhaust emissions. Therefore, Beijing's atmosphere has a strong aerosol concentration (Tang et al., 2016).

2.2. Data

2.2.1. MODIS level-2 AOD

The MODIS sensor is part of the 1991 NASA-initiated Earth observation system, which was established with the aims of monitoring the global environmental and climate change and observing and preventing large-scale natural disasters. The MODIS level-2 AOD data (C6) (10 km resolution) of the Beijing area for the entire calendar year of 2014 were collected from both the Terra and Aqua satellites in this study. The Terra satellite is timed to cross the equator from north to south at about 10:30 am local time, while the Aqua satellite is timed to cross the equator from south to north at about 1:30 pm local time. In this research, AOD products from the Terra and the Aqua satellites are labeled as AOD_{MOD} and AOD_{MYD}, respectively. The product can be obtained through a variety of free channels (https://ladsweb.nascom.nasa.gov/data/search.html), one of which was used as a data source for this study (Ma et al., 2014). ENVI IDL programs were developed to read the MODIS HDF files and to extract the AOD at 550 nm over land.

2.2.2. AERONET

The AERONET AOD observation data were obtained from https://aeronet.gsfc.nasa.gov/.html. There are two sites in Beijing (Fig. 1). The AERONET aerosol product includes three levels of datasets (level 1, level 1.5, and level 2). The level 1 products are unprocessed data, the level 1.5 products are cloud-screened data, and the level 2 products are quality assured data (Singh et al., 2016). The level 2 data were used in this research. Because the AERONET site does not contain the AOD in a 550 nm band, we derived the AERONET AOD values at 550 nm by interpolating the AOD in 440 nm and 675 nm bands to be compatible with MODIS AOD products using the following equation (Liu et al., 2004).

$$\tau_{550} = \tau_{\lambda 2} \times \left(\frac{\lambda 3}{\lambda 2}\right)^{-\alpha_{\lambda 1 \sim \lambda 2}}$$
$$\alpha_{\lambda 1 \sim \lambda 2} = -\frac{\ln(\tau_{\lambda 1}/\tau_{\lambda 2})}{\ln(\lambda 1/\lambda 2)}, \quad (1)$$

where $\tau_{\lambda 1}$ and $\tau_{\lambda 2}$ are AOD values at the wavelengths of λ1 (440 nm) and λ2 (675 nm). The spectral interpolation and extraction processes of the AERONET data were batch processed using R software.

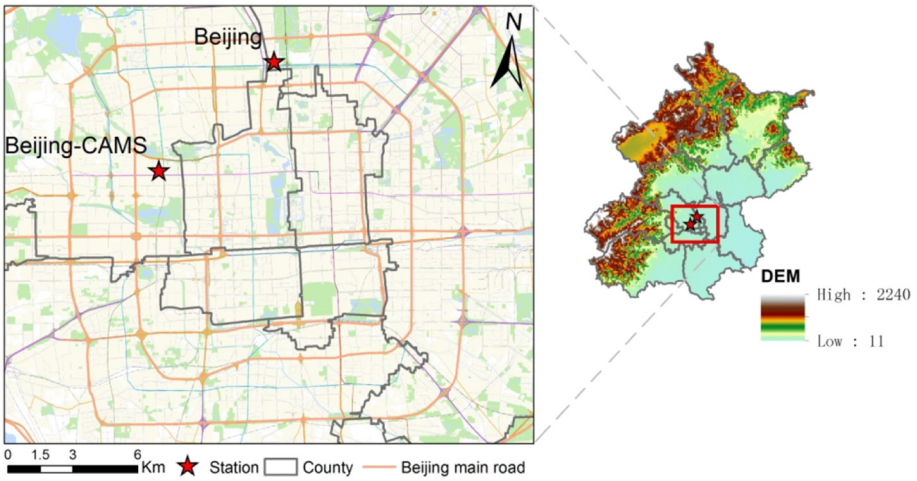

Fig. 1. The distribution of AERONET stations in Beijing.

2.3. Methodology

2.3.1. MODIS AOD calibration by AERONET

After extraction of MODIS AOD data in the study area, we calibrated the MODIS AOD value by the AOD data from AERONET. Satellite inversion AOD has a different resolution than ground monitoring data, and we cannot compare these two datasets directly. In this study, we adopted Liu et al.'s (2004) method to calculate the average of the satellite inversion data in the 0.5° × 0.5°border around the ground monitoring sites. Daily average AOD data from AERONET were used in the calibration due to the large amount of missing data. A simple linear regression model between MODIS AOD and AERONET AOD was developed (2):

$$AOD_{AERONET} = a + bAOD_{MODIS}, \tag{2}$$

where $AOD_{AERONET}$ refers to ground-based observations of AOD from AERONET, and AOD_{MOD} and AOD_{MYD} refer to AOD data from MODIS Terra and Aqua, respectively.

2.3.2. Spatiotemporal kriging

Kriging is a commonly used interpolation method in spatial analysis. It interprets geographic phenomena using a specific random process and obtains the best linear unbiased estimator under a second-order stationary assumption (Isaaks and Srivastava, 1989). Although kriging was originally applied in two- or three-dimensional space, spatiotemporal extensions of the method were proposed as early as in the 1990s due to the need for spatial and temporal data analysis in environmental studies, agriculture, and meteorology (Bogaert, 1996; Christakos and Hristopulos, 1998; Stein et al., 1998; Kyriakidis and Journel, 1999). The extension can be achieved by generalizing the traditional assumption of the spatial domain to the spatio-temporal domain, in which spatiotemporal covariance modelling is one of the most important parts (Porcu et al., 2006; Tilmann et al., 2006). Kyriakidis and Journel (1999) summarized the spatio-temporal models and classified the models into two conceptual viewpoints: one is the spatio-temporal random function model, which can be decomposed into a trend and a stationary residual component, and the other is the multiple vectors of spatial random function or vectors of time series. Hengl et al. (2012) built an ST model to interpolate daily mean temperatures over a year, which encouraged researchers to generate detailed daily maps of climatic variables by ST instead of using purely static models. Enkhtur (2013) applied spatiotemporal geostatistical methods to model and map air pollution data.

Similar to the spatial kriging, the spatiotemporal random process can be expressed by $Z = \{Z(s,t);\ s \in S,\ t \in T\}$, where $Z(s,t)$ is the observation of AOD at location s and at n time series t,

$$Z(s,t) = [Z_s(t)] = [Z_{s1}(t), \ldots, Z_{sn}(t)]' = [Z_1(t), \ldots, Z_n(t)]', \tag{3}$$

where $Z(s,t)$ is the random function in space S and time T, and s_j ($j = 1, \ldots n$) refers to spatial observation points. If $Z(s,t)$ has finite variance at all space-time locations, then the mean function $\mu(s,t) = E(Z(s,t))$ and the covariance between $Z(s,t)$ and $Z(s + h_s, t + h_t)$ exist and the spatiotemporal kriging predictor of $Z(s_0,t_0)$ is a linear combination (Gneiting, 2002):

$$\hat{Z}(s_0,t_0) = \mu(s_0,t_0) + \sum_{i=1}^{k} w_i(Z(s_i,t_i) - \mu(s_i,t_i)), \tag{4}$$

where w_i refers to weight of the ith available observation in $Z(s_i,t_i)$, which is solved using a covariance matrix equation. If the second-order stationary assumption is satisfied, then the covariance, C_{ST}, between two spatiotemporal points, $Z(s,t)$ and $Z(s + h_s, t + h_t)$, is defined as follows:

$$C_{ST}(h_s,h_t) = Cov(Z(s + h_s, t + h_t) - Z(s,t)), \tag{5}$$

where Cov is the covariance function, and h_s, and $h_t$represent the spatial and temporal intervals, respectively. Then, the variance of the predictor is obtained from the following equation:

$$Var\left(\hat{Z}(s_0,t_0)\right) = \sum_{i=1}^{k}\sum_{j=1}^{k} w_i w_j C(s_i - s_j, t_i - t_j) \tag{6}$$

Several types of spatiotemporal covariance models, including the metric model, product model, separable model, and sum-metric model, have been proposed in previous studies. In this study, we compared the four models and selected one of them based on minimum fitting error. The models differ in how the spatial and temporal correlations interact (De Cesare et al., 2001).

(1) Metric model: It is assumed that the spatial and temporal covariances are of the same type but possibly differ in terms of range:

$$C_{ST}(h_s,h_t) = C\left(\sqrt{\|h_s\|^2 + k\|h_t\|^2}\right), \tag{7}$$

where $\|h_s\|$ and $\|h_t\|$ are space and temporal distances, respectively. k is a geometric anisotropy parameter between space and temporal distances, which converts the time to the equivalent Euclidean space distance, with the same time and space lag from the different spatial distances and the length of time.

(2) Product model: One of the simplest ways to model spatiotemporal covariance is to separate the dependence from spatial domain and temporal domain. The product spatiotemporal covariance model is as follows:

$$C_{ST}(h_s, h_t) = C_S(h_s)C_T(h_t), \tag{8}$$

where $C_S(h_s)$ is the spatial covariance, and $C_T(h_t)$ is the temporal covariance.

(3) Separable model: For this model, the covariance matrices of certain configurations of spatiotemporal data are singular, and the covariance function is unsatisfactory for optimal prediction:

$$C_{ST}(h_s, h_t) = C_S(h_s) + C_T(h_t). \tag{9}$$

(4) Sum-metric model: This model is a combination of the spatial, temporal, and metric models and includes an anisotropy parameter: k. The sum-metric covariance model is as follows:

$$C_{ST}(h_s, h_t) = C_S(h_s) + C_T(h_t) + C_{ST}\left(\sqrt{\|h_s\|^2 + k\|h_t\|^2}\right), \tag{10}$$

where $C_{ST}(\sqrt{\|h_s\|^2 + k\|h_t\|^2})$ is the variance covariance function of the space and time interaction.

A semi-variogram is equivalent to a covariance function. The sum of the semi-variogram and the covariance function equals a constant (sill). In practice, instead of fitting a covariance function, we fitted a semi-variogram, as supported in the R gstat library. We compared the different models and determined which one had the best goodness of fit as measured by the mean fitting error.

2.3.3. Accuracy assessment

The interpolation accuracy was assessed by 10-fold cross validation. At first, the available pixels with AOD data were randomly separated into 10 parts of equal size. We repeated the interpolation process 10 times. At each time, one of the 10 parts was left out, and the remaining nine parts were used as known pixels to interpolate the left-out pixels. Two indices, mean absolute error (MAE) and root mean squared error (RMSE), were adopted to measure the cross-validation error. They are defined as Eqs. (11) and (12):

$$MAE = \sum_{i=1}^{n} | Y_i - \hat{Y}_i | /n \tag{11}$$

$$RMSE = \sqrt{\sum_{i=1}^{n} (Y_i - \hat{Y}_i)^2 /n}, \tag{12}$$

where Y_i and $Y_i\hat{}$ are the original i^{th} ($i = 1, \ldots, n$) data and the interpolated data, respectively.

3. Results

3.1. Data intercalibration

We compared the MODIS AOD products with AERONET at Beijing, Beijing-CAMS sites. There were 73 pairs of matched $AOD_{AERONET}$ and AOD_{MOD} records and 75 pairs of matched $AOD_{AERONET}$ and AOD_{MYD} records (Fig. 2). Exploratory data analysis results show that there is statistically significant correlation between MODIS AOD and AERONET AOD data. The correlation coefficient with MYD is 0.89, which is significantly higher than that with MOD (0.41). To ensure a high intercalibration result, we only selected MODIS MYD data and calibrated it using linear regression:

$$AOD_{AERONET} = -0.13 + 0.51 AOD_{MYD}, \tag{13}$$

where both the fitted interception and slope are statistically significant ($p < 0.01$).

3.2. Spatiotemporal modelling

Four models (separable, product, metric, sum-metric) were compared to fit the spatiotemporal experience variogram using the calibrated AOD_{MYD} data. When comparing the accuracy of the models to fit the experience semi-variogram from the available data, we adopted the MSE (mean-square error) as the comparative indicator. The MSE of the fitted result of the sum-metric variogram model is the smallest. Therefore, the fitting result of the sum-metric variogram model is closest to the real situations in the four models. The estimated spatiotemporal anisotropy parameter is about 14.130 km. The fitted sum-metric variogram model parameters are shown in Table 1. The fitted

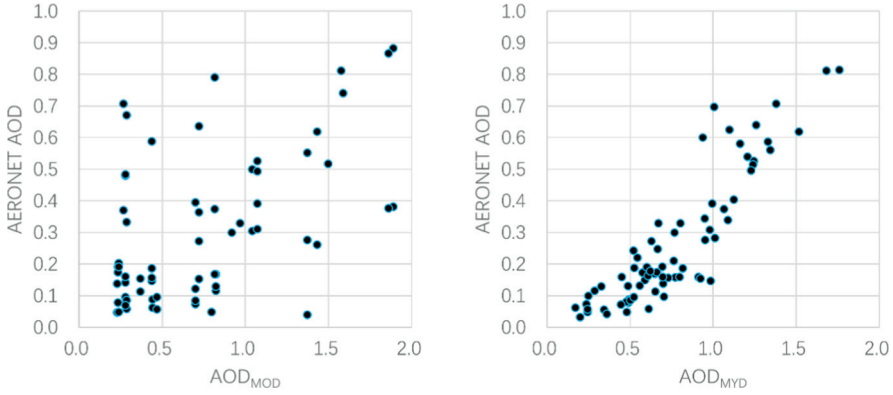

(a) $AOD_{MOD} \sim AOD_{AERONET}$ (b) $AOD_{MYD} \sim AOD_{AERONET}$

Fig. 2. Scatter plot between AERONET and MODIS AOD.

Table 1
Fitted spatiotemporal sum-metric variogram model.

Component	Model	Nugget	Partial sill	Range
Space-time join	Gaussian	0.007	0.120	10^4 km
Space	Exponential	0.000	0.140	60 km
Time	Gaussian	0.007	0.034	3 days

parameters showed that both spatial and temporal autocorrelation exists in the spatiotemporal data, and the former is stronger than the latter.

Besides spatiotemporal kriging, ordinary spatial kriging interpolation was also used to compare performances. The spatial component of the sum-metric variogram model was entered into the ordinary kriging model. Predictors, whose standard deviations were as high as three times that of the corresponding predicted values, were removed in both models. Ten-fold cross-validation with both spatiotemporal kriging and ordinary spatial kriging were performed. The RMSE of the spatiotemporal cross-validation result is 0.07, which is lower than that of spatial ordinary kriging (0.09). The MAE of spatiotemporal cross-validation is 0.04, which is also lower than that of spatial ordinary kriging (0.05).

3.3. Assessment of the completeness of interpolated AOD

The completeness of each pixel during 2014 in the study area was quantitatively evaluated for the interpolated results. Before interpolation, pixel-level completeness of the inter-calibrated AOD_{MYD} ranged from 7.12%–23.83%. The city center has a relatively higher missing percent of data than the north and south area (Fig. 3). The pixel-level data completeness of the spatial-interpolated results ranges from about 25%–45%, while the pixel-level data completeness of the spatiotemporal interpolated results ranges from 50%–85%. On average, the mean completeness of all pixels of the spatiotemporal results is 67.3%, which is much higher than that of the spatial-interpolated results (33.3%).

The daily pixel-level completeness of the two interpolated results was also calculated, as shown in Fig. 4. The days with no valid AOD_{MYD} data cannot be interpolated by the spatial kriging method, while the spatiotemporal kriging may work because it can "borrow" data from adjacent days.

3.4. Regional AOD patterns

The monthly mean AOD from spatiotemporal interpolation for the study region in 2014 is shown in Fig. 5. There are some data gaps in Jan, Feb, and Dec, and the data gaps are mainly distributed throughout the urban area of Beijing. The spatial distribution of AOD was low in the northwest and high in the southeast of the main city. There are two peaks in April and July, with clear monthly variation characteristics, and the monthly mean value ranges from −0.12–0.54. Summer is the highest season for AOD in the entire year: the monthly mean values of AOD in June, July, and August were 0.24, 0.35, and 0.26. AOD is high in summer, which is due to the burning of straw in summer farmland and high temperatures, which promote the accumulation of aerosols. Dust aerosol is an important source of atmospheric aerosols, and the high frequency of dusty days led to a significant increase of AOD value. In April, the monthly mean value of AOD was 0.24, due to a strong sand and dust weather invasion in Beijing; this led to dust aerosols, which accounted for the dominant part of atmospheric aerosols. As shown in Fig. 5, the AOD value in November was significantly lower than in October. On the whole, the time trend of AOD in Beijing reveals a seasonal pattern that was high in the spring and summer and low in the autumn and winter. This conclusion is consistent with conclusions from the existing literature (Qi et al., 2013).

The annual average AOD from spatiotemporal interpolation is overlaid on the Beijing County map (Fig. 6), which shows the distribution of Beijing ring roads and the location of the surrounding towns. The average AOD values in Beijing were in the range of 0.27–0.67 in 2014. We calculated the annual average AOD of each district in Beijing. The annual average AOD values that were >0.5 are mainly concentrated in the eastern part of the Chaoyang District and in the western part of the Tongzhou District, which is north of the Daxing District. The variation of the spatial distribution of AOD is mainly related to terrain and population activities. For example, in the western and northern sububs of Beijing, the elevation is rather high, and there is a significant amount of low-value AOD areas, as shown in Fig. 6. In downtown Beijing, where the area has a flat terrain and dense population activity, the AOD values are higher than in other areas of the city.

4. Discussion

As the spatiotemporal coverage and accuracy of AOD is important in the aerosol applications in climatological and environmental health studies, a geostatistical data interpolation framework based on the spatiotemporal kriging method was developed for interpolating satellite AOD products. The advantages of the presented merging framework are that it not only utilizes the spatial and temporal autocorrelations but also simultaneously considers the spatiotemporal autocorrelations, which can significantly improve the spatiotemporal coverage and accuracy of AOD. The results of the interpolation were compared with those of the spatial ordinary kriging interpolation method. Both the cross-validation result and pixel-level completeness statistics show that temporal autocorrelation is a useful characteristic of AOD in improving interpolation performance.

Beijing air pollution incidents mainly occur in the spring and winter. Fig. 5 shows that the monthly AOD trend is synchronized with the non-heating season and heating season. The heating season is from November 15 to March 14, in which the monthly average of AOD is generally

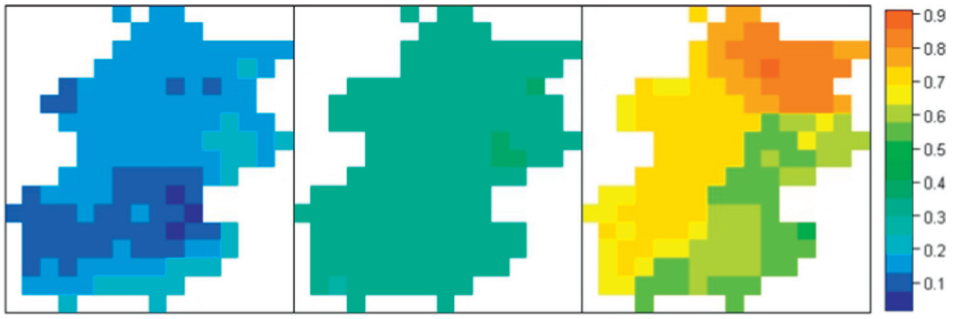

(a) no interpolation (b) after spatial interpolation (c) after spatiotemporal interpolation

Fig. 3. Comparison of spatial completeness of the original inter-calibrated AOD_{MYD}: spatial-interpolated and spatiotemporal-interpolated results.

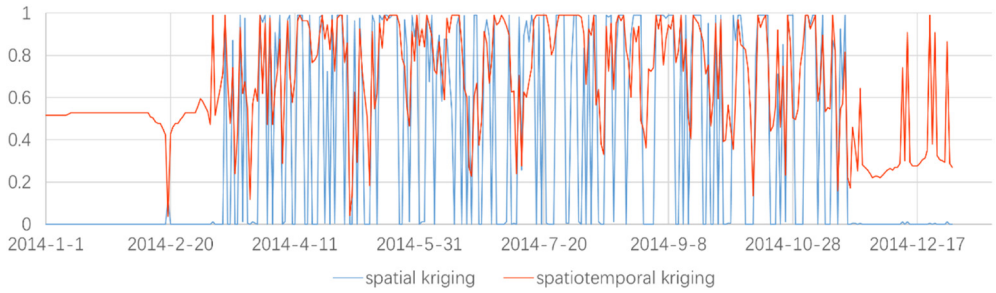

Fig. 4. The daily temporal completeness of the spatial-interpolated and spatiotemporal-interpolated AOD results.

low. The non-heating season is from March 15 to November 14, in which the monthly average of AOD is relatively higher than that of the heating season. The weather in spring is dominated by dust. The statistics show that from 2000 to 2010, major dust-type pollution occurred 53 times, followed by 15 more events in 2010. Beijing suffered from an invasion of Inner Mongolia dust, leading to soaring values on the Beijing AQI index; moreover, an aerosol haze appeared and remained for a long time, and the level of visibility was <10 km on April 10, 2014. The AOD monthly average in April was the highest during the year, which is consistent with conclusions from existing literature (Chen et al., 2016; Qi et al., 2013; Xi and Sokolik, 2016).

In summer, because biomass combustion is particularly evident and the vertical direction of turbulence is strong, more particles are sent to high altitudes. Based on Beijing meteorological data, most of the weather in July is cloudy or rainy, with 3 to 4 grades of southwest wind, and the polluted particles are mainly derived from regional transmissions in the southwestern part of Beijing. Moreover, with the arrival of the rainy season, the water vapor in the air increases, which causes an increase in AOD in the entire atmosphere and affects the shapes and radiation values of the aerosol particles (Singh et al., 2016). At the APEC meeting held in Beijing in November, the government adopted a series of measures to control air pollution and to ensure good air quality. According to the Ministry of Environmental Protection, historical data show that the air quality was excellent in Beijing during the APEC meeting period (November 1–12), which was reflected by the low monthly mean value of AOD in November. As coal-fired heating occurs in winter, the air particles significantly increase, visibility decreases, and air quality decreases. The satellite inversion AOD algorithm cannot distinguish between aerosol particles and clouds; thus, several data gaps appear. Because the satellite inversion AOD only records the good weather during the winter, the monthly mean AOD is relatively low during this period.

The spatial variations of AOD in Beijing may be related to topography (Zhang et al., 2013). The Beijing plain is surrounded by the Taihang Mountains in the west and the Yanshan Mountains in the north. These two mountain ranges form a “dustpan” pocket. Beijing's air pollutants mainly come from the southwest (Hebei Baoding) and the city's own emissions (Li et al., 2003). Through the dominant south wind, the pollutants are transported from the south to the Beijing urban area and spread over the eastern plain of Beijing. Therefore, the high value of average annual AOD is mainly concentrated in the middle of the Beijing plain, and the low value is mainly concentrated in the northern higher

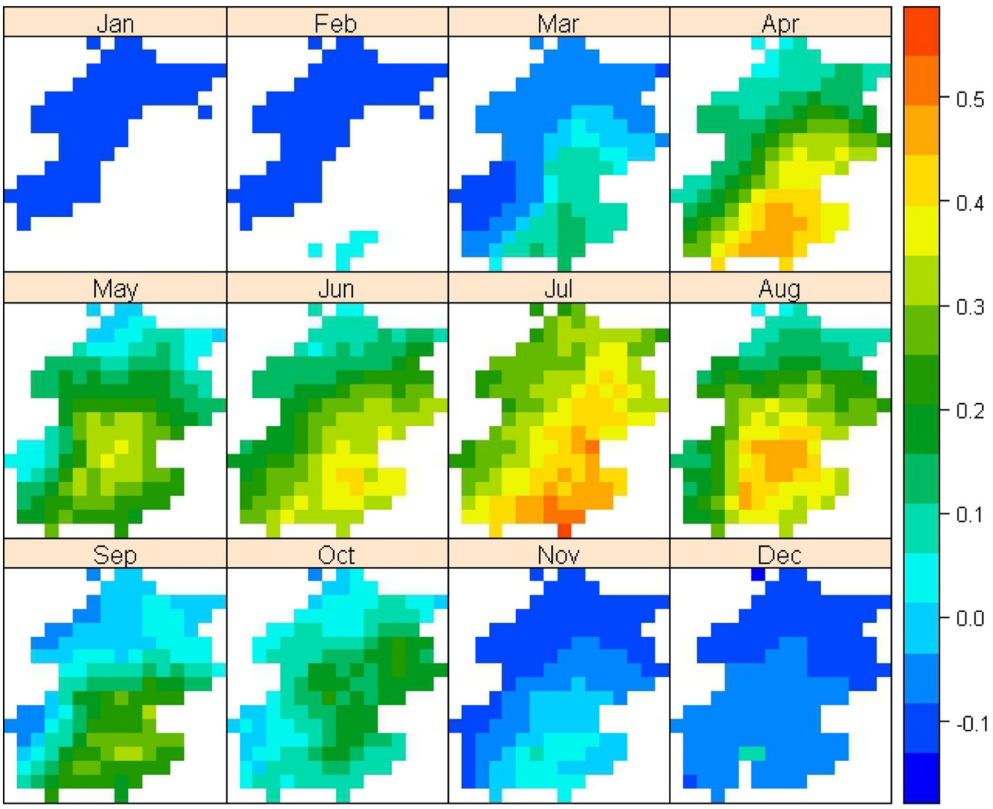

Fig. 5. Monthly average AOD from spatiotemporal kriging interpolation in Beijing, 2014.

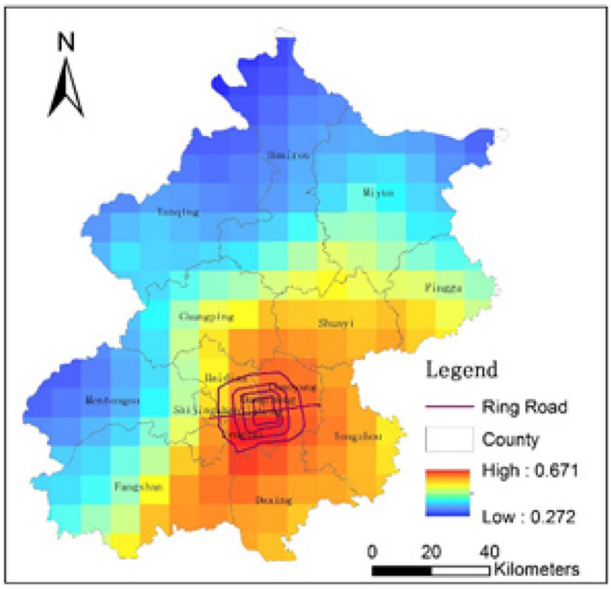

Fig. 6. The distribution of the annual average of spatiotemporal-interpolated AOD in Beijing 2014.

mountains. These results confirm that the areas with large AOD values are basically distributed in the middle plain areas and that the lower AOD values are concentrated in the northern mountainous suburbs.

Although the spatiotemporal interpolation method performs well in terms of AOD gap filling by considering both spatial and temporal autocorrelations, there are also some limitations in the study. The performance of the presented interpolation method depends on the observation availability of the MODIS level-2 AOD data. In the area where neighboring spatial and temporal radium measurements have large data gaps, insufficient observations may lead to physically unrealistic features in the interpolated AOD. More auxiliary data with higher completeness may be helpful for improving the model's performance.

5. Conclusion

This study proposed a daily MODIS level-2 AOD gap-filling method based on the spatiotemporal kriging model. Using a 10-fold cross-validation method, the method performed better in presenting spatiotemporal variations and improving the data completeness and stability than the spatial ordinary kriging. According to the interpolation results, we found that the AOD distribution in Beijing had typical seasonal variations that were highly related to topography. The low-altitude plain areas in the spring and summer are have high-value concentrations of AOD, while the high-altitude suburbs in the autumn and winter have low-value concentrations of AOD.

Acknowledgments

This work was supported by the National Natural Science Foundation of China (Nos. 41771434, 41531179) and a grant from the State Key Laboratory of Resource and Environment Information System (No. O88RA200YA).

References

Bogaert, P., 1996. Comparison of kriging techniques in a space-time context. J. Math. Geol. 28 (1), 73–86.
Chatterjee, A., Michalak, A.M., Kahn, R.A., Paradise, S.R., Braverman, A.J., Miller, C.E., 2010. A geostatistical data fusion technique for merging remote sensing and ground-based observations of aerosol optical thickness. J. Geophys. Res. Atmos. 115 (D20), D20207.
Chen, D., Tian, J., 2010. Monitoring spatial and temporal variability of air quality using satellite observation data: a case study of MODIS-observed aerosols in Southern Ontario, Canada. INTECH Open Access Publisher ISBN 9533071311, 9789533071312.
Chen, W., Tang, H., Zhao, H., Yan, L., 2016. Analysis of aerosol properties in Beijing based on ground-based sun photometer and air quality monitoring observations from 2005 to 2014. Remote Sens. 8 (2), 110.
Chin, M., 2009. Atmospheric Aerosol Properties and Climate Impacts. DIANE Publishing.
Christakos, G., Hristopulos, D., 1998. Spatiotemporal Environmental Health Modelling. Kluwer Academic Publishers.
De Cesare, L., Myers, D., Posa, D., 2001. Estimating and modeling space–time correlation structures. Stat. Probab. Lett. 51 (1), 9–14.
Enkhtur, B., 2013. Geostatistical Modelling and Mapping of Air Pollution. University of Twente Faculty of Geo-Information and Earth Observation (ITC).
Flato, G., Marotzke, J., Abiodun, B., Braconnot, P., Chou, S.C., Collins, W.J., Eyring, V., 2013. Evaluation of climate models. In: climate change 2013: the physical science basis. Contribution of working group I to the fifth assessment report of the intergovernmental panel on climate change. Climate Change 5, 741–866.
Gneiting, G., 2002. Nonseparable, stationary covariance functions for space-time data. J. Am. Stat. Assoc. 97 (458), 590–600.
Hengl, T., Heuvelink, G.B., Tadić, M.P., Pebesma, E.J., 2012. Spatio-temporal prediction of daily temperatures using time-series of MODIS LST images. Theor. Appl. Climatol. 107 (1–2), 265–277.
Isaaks, E., Srivastava, R., 1989. Applied Geostatistics. Oxford University Press.
Kokhanovsky, A., Breon, F.M., Cacciari, A., Carboni, E., Diner, D., Di Nicolantonio, W., Lee, K. H., 2007. Aerosol remote sensing over land: a comparison of satellite retrievals using different algorithms and instruments. Atmos. Res. 85 (3), 372–394.
Kyriakidis, P., Journel, A., 1999. Geostatistical space–time models: a review. Math. Geol. 31 (6), 651–684.
Li, C., Mao, J., Lau, K.H.A., et al., 2003. Characteristics of distribution and seasonal variation of aerosol optical depth in eastern China with MODIS products. J. Chin. Sci. Bull. 48 (22), 2488–2495.
Liu, Y., Sarnat, J.A., Coull, B.A., Koutrakis, P., Jacob, D.J., 2004. Validation of multiangle imaging spectroradiometer (MISR) aerosol optical thickness measurements using Aerosol Robotic Network (AERONET) observations over the contiguous United States. J. Geophys. Res. Atmos. 109 (D6), D06205.
Ma, Z., Hu, X., Huang, L., Bi, J., Liu, Y., 2014. Estimating ground-level PM2. 5 in China using satellite remote sensing. Environ. Sci. Technol. 48 (13), 7436–7444.
Papadimas, C., Hatzianastassiou, N., Mihalopoulos, N., Querol, X., Vardavas, I., 2008. Spatial and temporal variability in aerosol properties over the Mediterranean basin based on 6-year (2000–2006) MODIS data. J. Geophys. Res. Atmos. 113 (D11), D11205.
Porcu, E., Gregori, P., Mateu, J., 2006. Nonseparable stationary anisotropic space–time covariance functions. Stoch. Env. Res. Risk A. 21 (2), 113–122.
Qi, Y., Ge, J., Huang, J., 2013. Spatial and temporal distribution of MODIS and MISR aerosol optical depth over northern China and comparison with AERONET. Chin. Sci. Bull. 58 (20), 2497–2506.
Ramachandran, S., 2007. Aerosol optical depth and fine mode fraction variations deduced from moderate resolution imaging spectroradiometer (MODIS) over four urban areas in India. J. Geophys. Res. 112 (D12), D16207.
Remer, L.A., Kaufman, Y., Tanré, D., Mattoo, S., Chu, D., Martins, J.V., Kleidman, R., 2005. The MODIS aerosol algorithm, products, and validation. J. Atmos. Sci. 62 (4), 947–973.
Ruiz-Arias, J., Dudhia, J., Lara-Fanego, V., Pozo-Vázquez, D., 2013. A geostatistical approach for producing daily Level-3 MODIS aerosol optical depth analyses. Atmos. Environ. 79, 395–405.
Sahoo, T., Patnaik, S., 2008. Cloud removal from satellite images using auto associative neural network and stationary wevlet transform. International Conference on Emerging Trends in Engineering and Technology, p. 2008.
Singh, M.K., Gautam, R., Venkatachalam, P., 2016. A merged aerosol dataset based on MODIS and MISR aerosol optical depth products. Paper Presented at the SPIE Asia-Pacific Remote Sensing.
Stein, A., Van Groenigen, J., Jeger, M., Hoosbeek, M., 1998. Space-time statistics for environmental and agricultural related phenomena. Environ. Ecol. Stat. 5 (2), 155–172.
Tang, Q., Bo, Y., Zhu, Y., 2016. Spatiotemporal fusion of multiple-satellite aerosol optical depth (AOD) products using Bayesian maximum entropy method. J. Geophys. Res. Atmos. 121 (8), 4034–4048.
Tilmann, G., Marc, G., Peter, G., 2006. Geostatistical space-time models, stationarity, separability, and full symmetry. In: Finkerstadt, B., Held, L., Isham, V. (Eds.), Statistical Methods for Spatio-temporal Systems. Chapman and Hall/CRC.
Van Donkelaar, A., Martin, R.V., Brauer, M., Kahn, R., Levy, R., Verduzco, C., Villeneuve, P.J., 2010. Global estimates of ambient fine particulate matter concentrations from satellite-based aerosol optical depth: development and application. Environ. Health Perspect. 118 (6), 847.
Xi, X., Sokolik, I.N., 2016. Dust interannual variability and trend in Central Asia from 2000 to 2014 and their climatic linkages. J. Geophys. Res. Atmos. 120 (23), 12175–12197.
Zhang, J., Wu, L., 2018. The influence of population movements on the urban relative humidity of Beijing during the Chinese Spring Festival holiday. J. Clean. Prod. 170, 1508–1513.
Zhang, A., Qi, Q., Jiang, L., Zhou, F., Wang, J., 2013. Population exposure to PM2.5in the urban area of Beijing. PLoS One 8 (5), e63486.